Reports on Progress in Physics

Check for updates

RECEIVED
22 July 2026

REVISED
26 August 2026

ACCEPTED FOR PUBLICATION
11 September 2026

PUBLISHED
12 October 2026

PAPER

Percolation dissipation of the α and β processes in metallic glasses

Sheng-Hao Zeng[1,4], **Bo-Yan Wang**[1,4], **Liang Gao**[1,4], **Qun Yang**[2], **Jun-Ying Jiang**[1], **Zi-Yi Ren**[1], **Jeppe C Dyre**[3] **and Hai-Bin Yu**[1,*]

[1] Wuhan National High Magnetic Field Center and School of Physics, Huazhong University of Science and Technology, Wuhan, Hubei 430074, People's Republic of China
[2] College of Physics and Electronic Engineering, Chongqing Normal University, Chongqing 401331, People's Republic of China
[3] Glass and Time, IMFUFA, Department of Science and Environment, Roskilde University, DK-4000 Roskilde, Denmark
[4] These authors contributed equally.
[*] Author to whom any correspondence should be addressed.

E-mail: haibinyu@hust.edu.cn

Keywords: metallic glasses, α relaxation, β relaxation, double-percolation, relaxation dissipation

Supplementary material for this article is available online

Corresponding editor: Dr Lorna Brigham

Abstract

Dynamic processes in glasses are crucial for unraveling fundamentals of the glass transition and material properties. A recent theoretical framework proposes a 'double-percolation' scenario for the α and β-relaxation processes. While supported by simulations, no experimental validation has so far been presented. We here conduct a comprehensive analysis of the relaxation dissipation of more than 300 mechanical spectra of metallic glass samples. Our study yields two key findings, both aligning with the double-percolation theory: (i) The α-relaxation has a damping factor of 0.6 ($\pm$0.05), independent of material composition, probing frequency, and thermal history—a signature that is consistent with the percolation of immobile atomic clusters proposed to characterize the α-relaxation. (ii) The β-relaxation dissipation, though of variable magnitude and dependent on external factors, can be rationalized as caused by the percolation of mobile atomic entities driving configurational rearrangements; thus for the β-relaxation we show that certain atomic motions are neither dissipative nor induce configurational changes. These results bridge theoretical predictions with experimental observations, suggesting a generally applicable picture of the atomic-scale mechanisms of relaxation dissipation in glass formers.

1. Introduction

Amorphous and glassy materials are essential for modern technologies, but understanding the structure-property relationship remains a significant challenge for solid-state physics and materials science [1–6]. Unlike crystalline materials, which have well-defined phonon and defect dynamics, glassy materials exhibit complex relaxation processes across all temperatures and timescales [2, 7–13]. As liquids cool towards the glass transition, flow occurs on extremely long timescales, independent of atomic details and chemical composition [14–21]. Additional processes, such as the β-relaxation, excess wing and nearly constant loss, emerge at further cooling. At the atomic level, these dynamics are governed by a complex hierarchy of relaxation processes that are challenging to reconcile into a coherent framework [2, 7, 8, 22, 23].

Recently, a unified 'double-percolation' description for the mechanical response has been proposed [24–30]. As shown schematically in figure 1(a) giving the mechanical loss at a fixed frequency upon cooling from the liquid state, percolation of immobile particles identifies the α process. Further cooling into the glass state leads to a mobile-particle percolation transition, which has been identified as the β process [8, 24, 31–33] , often described in terms of subdiffusive motion, particle jumps, collective small displacements, and nanomechanical heterogeneities [34–37]. The 'double-percolation' framework offers a

© 2026 IOP Publishing Ltd. All rights, including for text and data mining, AI training, and similar technologies, are reserved.

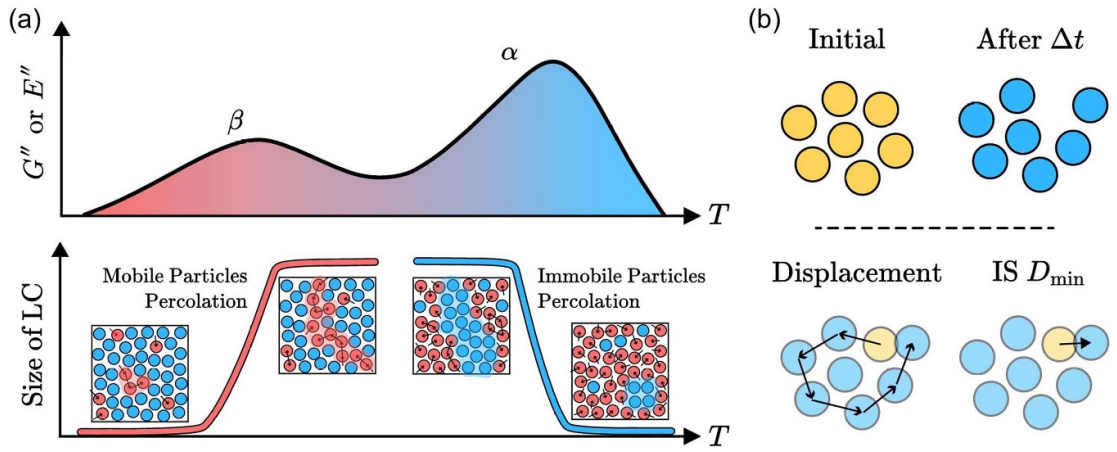

Figure 1. Schematic diagram of the sources of relaxation dissipation as observed for cooling through the glass transition during which the mechanical loss modulus (simulated, G'' and experimental, E''; see Methods for details). (a) Relaxation dissipation (upper panel) and double-percolation (lower panel). LC means the largest cluster in the percolation cluster analysis. (b) Illustration of the difference between labeled displacement and the actual configuration change, IS $D_{\min}$ [47].

Table 1. Overview of the metallic glasses studied; more details can be found in the supplementary information.

Systems	Number of compositions	Number of spectra
La-MGs	32	85
Pd-MGs	9	56
Zr-MGs	21	25
Y-MGs	19	58
Dy-MGs	19	39
Ce-MGs	16	18
Mg-MGs	1	5
Simulations	7	30
Others(from literature)	20	20
Summary	144	336

general description of glassy dynamics that incorporates well-established factors such as dynamic heterogeneity and facilitation [25, 38–45]. However, the double-percolation framework currently only relies on molecular dynamics (MD) simulations resolving the atomic motion at sub-nanosecond timescales [26, 29, 46], and the question is to which degree this scenario applies to real-world materials.

Yu *et al* recently established a global configuration-based correlation between the inherent structure (IS) minimal displacement, IS$D_{\min}$, and the system dissipation, $\tan\delta$, expressed as $\tan\delta \propto (\mathrm{IS}D_{\min})^b$ [47, 48]. From a potential-energy-landscape (PEL) perspective, IS$D_{\min}$ describes the shortest distance between neighboring IS; it governs the activation barrier for transitions between PEL local minima and thereby dictates the mechanical dissipation.

In this study, we bridge the theory-experiment gap by analyzing the relaxation dissipation of more than 300 metallic glass (MG) samples collected over a decade (2016–2025) in our laboratory, as well as from literature (the relevant data can be found in table 1 and figures S1–S22). One connection between the theory of double-percolation and experiments is that the theory predicts immobile-particle percolation that involves about 25% of the atoms during α-relaxation, while the mobile-particle percolation involves about 10% of the atoms (controlling the β-relaxation). This implies that the two relaxation dissipations should be universally constant if one assumes that all the mobile atoms contribute to the dissipation. We show below that the α-relaxation is fully consistent with this expectation, as the damping factor reaches about 0.6 regardless of chemical composition and thermal history. While the dissipation of the β process does depend on these factors, we argue that this does not invalidate mobile-particle percolation as a β-relaxation characteristic. This is confirmed by our finding that a sample-preparation-dependent portion of atomic motions are not effective in changing configuration and thus much less dissipative, compare the illustration in figure 1(b).

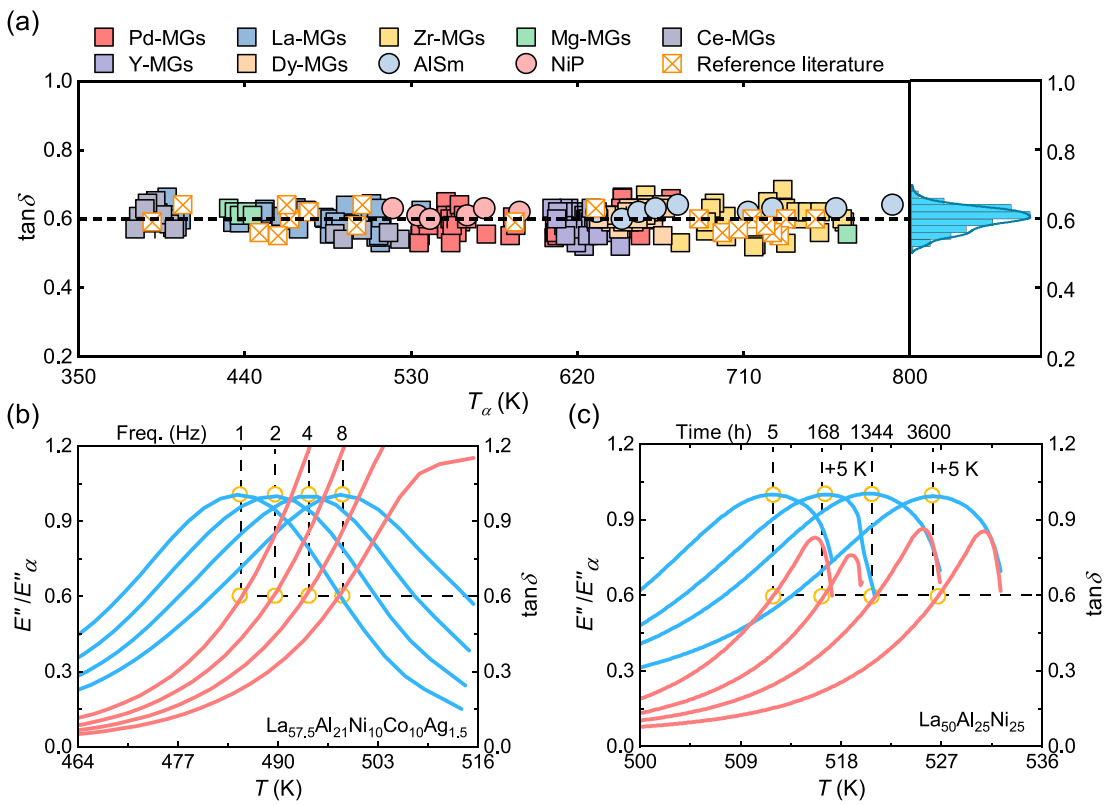

Figure 2. Dissipation of the α-relaxation. (a) The loss tanδ at the temperature corresponding to the α peaks of different metallic glasses, including experimentally measured Pd-MGs, La-MGs, Zr-MGs, Y-MGs, Mg-MGs, Ce-MGs, and Dy-MGs, simulated AlSm and NiP, and tanδ data from other references. Solid squares represent experimental data and filled circles simulation results, while open squares represent literature data. The histogram gives the statistical distribution of tanδ, showing that tanδ dominantly is between 0.55 and 0.65. (b) The loss modulus and tanδ measured at different frequencies for $La_{57.5}Al_{21}Ni_{10}Co_{10}Ag_{1.5}$ MG. (c) The loss modulus (blue) and tanδ (red) curves for $La_{50}Al_{25}Ni_{25}$ annealed at 373 K for 5 h, 168 h, 1344 h, and 3600 h.

2. Results

2.1. Dissipation of α relaxation

Figure 2(a) summarizes the dissipation associated with the α-relaxation in terms of the damping factor tanδ, measured by dynamic mechanical spectroscopy (DMS). As illustrated in figures 2(b) and S23–S25, tanδ of α-relaxation is determined at the peak position of loss modulus E'' monitored at a fixed frequency during heating at a constant rate. Our dataset encompasses nine different groups of MGs with distinct base elements, featuring glass transition temperatures ranging from 400–800 K. Notably, the samples exhibit nearly constant tanδ values of 0.6 ± 0.05, with no systematic deviations. In particular, figure 2(c) demonstrates that extended-time aging does not affect the constant tanδ behavior, further confirming the robustness of this finding. According to the Kohlrausch–Williams–Watts stretched exponential equation, the theoretical maximum of $\tan\delta$ is approximately 0.67 for $\beta = 0.5$, which is close to the experimentally observed (details are given in the supplementary information–2).

The universal dissipation of the α-relaxation can be interpreted as a direct reflection of the percolation of immobile atoms [25, 26]. The α-relaxation takes place at the emergence of a percolating cluster of immobile atoms, i.e. atoms that over the characteristic α-relaxation time scale do not jump longer than half the mean interatomic distance. The percolation threshold is found where about 25% of the atoms are immobile while the remaining roughly 75% exhibit large diffusive motions [24–26].

2.2. Dissipation of the β relaxation

Figure 3(a) shows the dissipation of the β-relaxation. Here we find no constant tanδ, and the chemical composition has a notable effect on the loss magnitude. For example, most Pd-based MGs have large tanδ values between 0.04 and 0.08, while La-based MGs have values below 0.04. Moreover, as shown in figure 3(b), tanδ depends on the frequency (red curve). Finally, aging has a pronounced influence on tanδ of the β-relaxation (figure 3(c)). The effect of thermal history on β-relaxation has previously been investigated in various types of glassy materials [49, 50]. For instance, vapor-deposited ultrastable

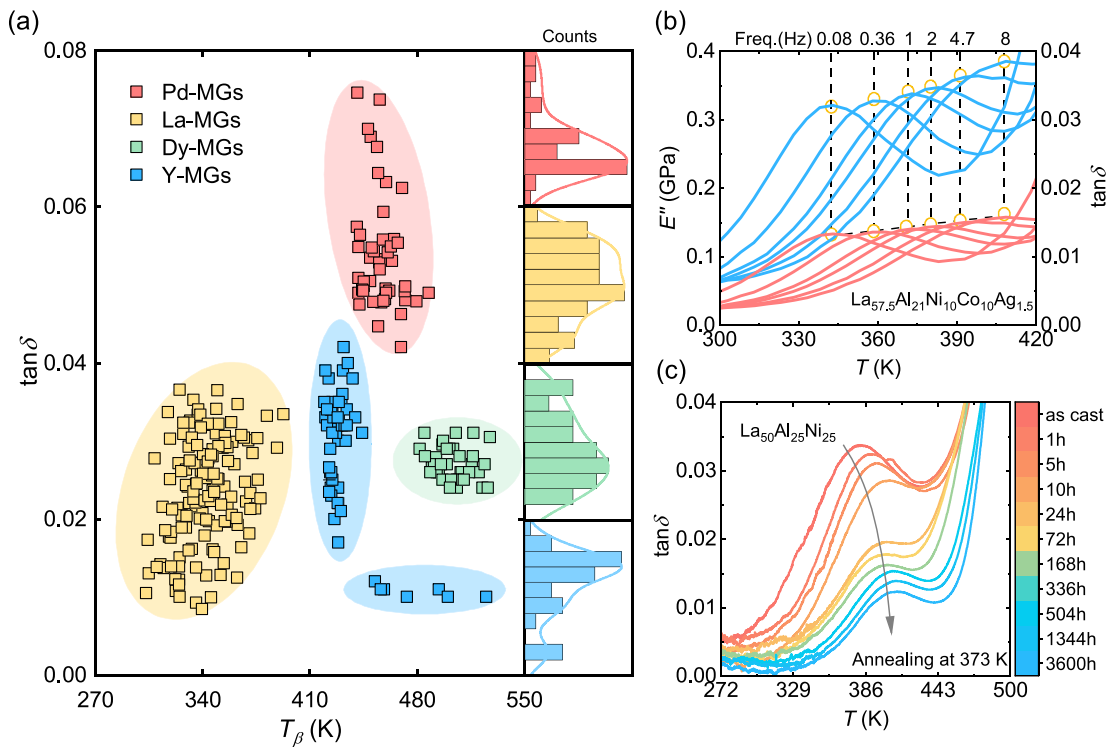

Figure 3. Dissipation of the β-relaxation. (a) tanδ of Pd-MGs (red), La-MGs (yellow), Dy-MGs (green), and Y-MGs (blue) systems, all of which exhibit well-defined β-relaxations. The right-hand panels show the distribution of the tanδ for each system. (b) Loss modulus E'' (blue) and tanδ (red) of the $La_{57.5}Al_{21}Ni_{10}Co_{10}Ag_{1.5}$ MG measured at different frequencies. (c) tanδ curves of $La_{50}Al_{25}Ni_{25}$ MG after annealing at 373 K for a range of times, from the as-cast state up to 3600 hours.

toluene glass exhibits a 70% suppression of β-relaxation, equivalent to approximately 3000 years of aging [51]. Likewise, in phase-change materials for memory applications the β-relaxation is highly tunable (which is fortunate because it enables tailoring the rate of crystallization [52]). Thus in contrast to the α-relaxation, the β-relaxation exhibits no universal dissipation.

2.3. Atomic motion and configuration variation

The above results raise questions about the validity of the universal double-percolation scenario in regard to the β-relaxation. Given that the percolation threshold for mobile percolation is always found at a constant fraction of 10%, one might expect tanδ of the β-relaxation to be universal [24, 26]. We now proceed to show why this is not the case.

As demonstrated recently, the relaxation dissipation tanδ has a scaling relationship with the configurational variation, as characterized by the 'inherent structural minimal displacement' (IS $D_{\min}$) [47]. Obviously, only atomic motions that change configurations will affect tanδ. Thus if sample-dependent motions exist that contribute to the percolation but do not - or hardly - change the configuration, the tanδ value of the β-relaxation will depend on the sample. We demonstrate that this is the case as follows.

In figure 4 we employ a combination of MD-DMS and percolation analysis to characterize the atomic motion within both the mobile and the immobile clusters. We find that for the β-relaxation, substantial motions are string-like wherein one particle moves into the position vacated by its neighbor in a sequential manner [53–56]. These diffusive motions contribute to the mobility percolation, but only result in minimal configurational changes (and no changes at all if identical elements are involved). A similar phenomenon does not apply for the α-relaxation, which in the double-percolation picture is characterized by the percolation of immobile particles.

To validate string-like motion as the underlying cause of the reduced β-relaxation observed as a consequence of aging, we performed two simulations resulting in, respectively, a rapidly quenched sample (fast-cooled) obtained by the cooling rate 100 K ns^{-1} and an aged sample (slow-cooled) from the cooling rate 0.1 K ns^{-1}. The latter exhibits a lower tendency for atomic motion, as shown in figure S31. To mimic experimental DMS measurements, both samples were subsequently reheated from 200–600 K (figure S26). Their loss-modulus spectra as functions of temperature at the frequency corresponding to

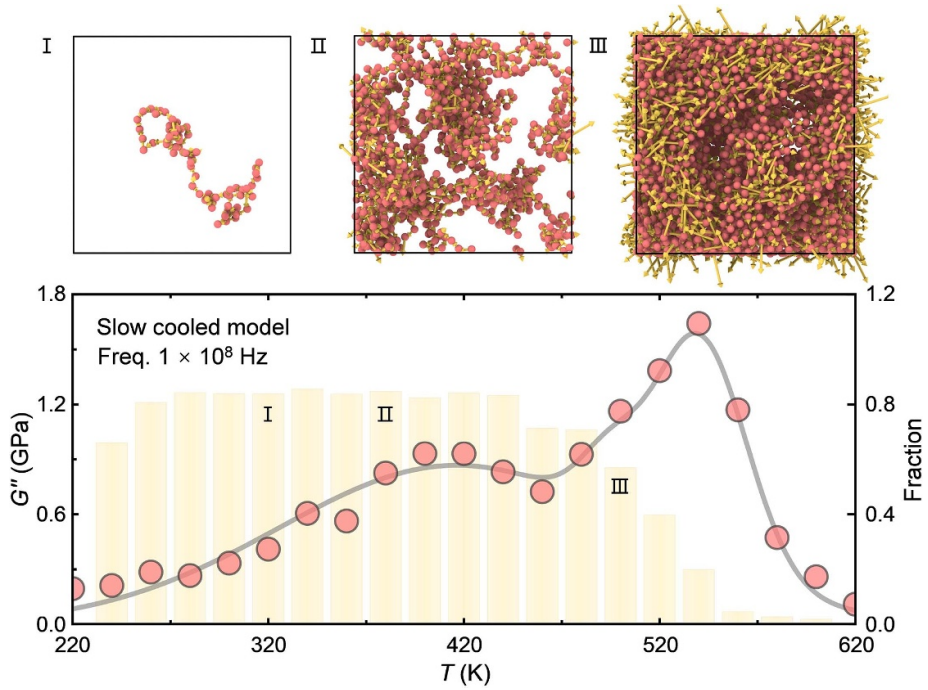

Figure 4. Relaxation dissipation and percolation-cluster analysis. The upper panels show the evolution of the largest cluster of mobile atoms at different temperatures. The lower panel represents the loss spectra obtained from MD-DMS calculations. The histogram represents the fraction of string-like atoms among mobile atoms.

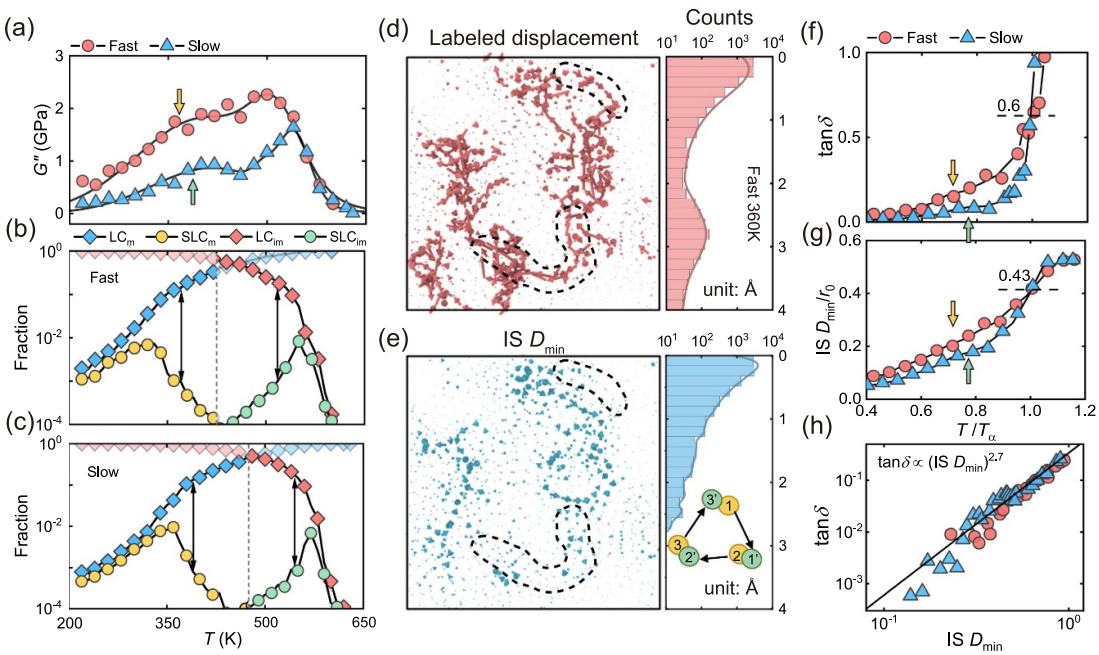

Figure 5. Double-percolation analysis and inherent-structure minimal displacement. (a) Loss spectra of $Al_{95}Sm_5$ model MGs prepared by fast (red, 100 K ns^{-1}) and slow (blue, 0.1 K ns^{-1}) cooling, calculated using MD-DMS. The positions of the β-relaxation are marked by yellow and green arrows, respectively. The mobile and immobile percolation analysis for (b) fast-cooled and (c) slow-cooled model MGs. 'LC' marks the largest cluster, 'SLC' the second-largest cluster. The left panels of (d) and (e) show the spatial manifestations of the labeled displacement (red) and the IS $D_{\min}$ (blue) at 360 K during DMS, respectively. The right panels present the corresponding statistical distributions. (f) tanδ and (g) IS $D_{\min}/r_0$ as functions of temperature relative to T_g for fast-cooled and slow-cooled model MGs. Here, r_0 is a typical length scale, defined as (Volume/Number of Atoms)$^{\frac{1}{3}}$. (h) Correlation between tanδ and IS $D_{\min}$, with a power-law exponent of 2.7.

the probing time $t_\omega = 10$ ns are presented in figure 5(a). We see that the fast-cooled sample exhibits a higher value of tanδ, consistent with experimental observations.

Figures 5(b) and (c) shows the corresponding double-percolation analysis, where the left side of each panel shows the behavior of the mobile atoms. As the temperature approaches the β-relaxation region,

the largest cluster (LC) rapidly expands by incorporating smaller, isolated clusters such as the second-LC (SLC), eventually spanning the entire configuration space. For both the fast and slowly cooled samples, β-relaxation occurs at their respective mobility percolations. Notably, both systems exhibit a 10% percolation threshold regardless of thermal history.

For the fast and slowly cooled samples, respectively, figures 5(d) and (e) compare the particle-labeled displacement $\Delta r_i(\Delta t) = r_i(\Delta t) - r_i(0)$ and the configuration displacement $r_{c,i}(\Delta t) = r_i(\Delta t) - Xr_j(0)$, respectively. Here the X is the permutation matrix (details on its definition and computations are given in the supporting information). The configuration displacement is defined without considering atomic labels [42], focusing solely on how atomic positions in space are occupied. The global parameter IS $D_{\min}$ is defined as [47]:

$$\mathrm{IS}\,D_{\min}(t) = \left[\frac{1}{N}\min\sum_{i,j}^{N,N} C_{ij}(t)\,X_{ij}(t)\right]^{1/2}. \tag{1}$$

In equation (1), $C_{i,j}(t) = \left[\vec{r_i}(t+t_0) - \vec{r_j}(t_0)\right]^2$ is the so-called *cost matrix* in which $\vec{r_i}$ is the position of the $i-$th atom and N is the number of atoms; X is a $N \times N$ boolean matrix, where $X[i,j] = 1$ if row i is assigned to column j for the minimization of equation (1) and otherwise $X[i,j] = 0$. This metric characterizes structural rearrangements by tracking the spatial occupancy of atoms rather than their individual identities, emphasizing the collective spatial redistribution of atomic configurations.

Clearly, some displacements in figure 5(d) do not result in a configuration change, as illustrated by the two dashed ring regions in figure 5(e). Figures 5(f) and (g) show tanδ and IS $D_{\min}$, respectively. We find that the slow-cooled MG model exhibits smaller IS $D_{\min}$ and tanδ, and a larger fraction of string-like motion (figures S27(c)). This is consistent with the arguments that only motions that change the configuration affect tanδ. Figure 5(h) shows that within the numerical uncertainty the IS $D_{\min}$ and $\tan\delta$ follow the same relation for the two models. Furthermore, the same analysis holds also for other glass models, including $Al_{90}Sm_{10}$, $Cu_{50}Zr_{50}$, $Ni_{65}Nb_{35}$, and $Ni_{80}P_{20}$, as documented in Supplementary figures S27–S30.

Our physical picture of the β-relaxation is that the majority of atoms remain immobile and only $\sim 10\%$ of them jump distances exceeding the interatomic spacing. These motions are collective in nature, with a subset displaying string-like behavior involving sequential position replacement. The string-like motions are inefficient at inducing configurational changes, which explains the low-loss character observed by DMS. This mechanism underscores the role of collective atomic rearrangements in mediating relaxation processes without substantial energy dissipation: *Only atomic motions that change configurations result in dissipation.*

Unlike the β-relaxation, where collective motions are largely configurationally inefficient, the α-relaxation is dominated by configurationally effective atomic rearrangements, resulting in the breaking of the percolating structure of immoble atoms. The extensive atomic mobility and the resulting large structural changes directly account for the strongly dissipative nature of the α-relaxation and its constant damping factor as shown in figures 2(a)–(c).

3. Discussion

We have shown that the α-relaxation in glasses exhibits a universal damping factor tanδ of 0.6 ± 0.05, independent of material composition, probing frequencies, and thermal history. This finding aligns with the double-percolation scenario in which the α-relaxation arises from the percolation of immobile atomic clusters involving about 25% of the atoms [25, 26], compare the right side of figures 5(b) and (c), while the remaining 75% atoms all contribute to relaxation dissipations. In contrast to the β-relaxation, the magnitude of the α-relaxation is virtually independent of the conditions of sample preparation. This is because the system is liquid above the α-relaxation, a phase that is fully characterized by pressure and temperature.

The β-relaxation dissipation, on the other hand, depends on external factors. Yet this variability can also be rationalized by the double-percolation scenario [57]. Here, a subset of diffusive atomic motions shows string-like behavior, contributing to mobility percolation without inducing significant configurational changes. This explains the non-constant tanδ of the β-relaxation [54, 58, 59]. As a consequence, the reduction of β-relaxation dissipation observed in annealed compared to vapor-deposited ultrastable

glasses stems not only from reduced atomic mobility, but also from an enhancement of low-loss motions [49–51].

Furthermore, β-relaxation shares an identical physical origin with the recently identified subdiffusive motion, particle jumps, collective small displacements and nanomechanical heterogeneities—all arising from percolating configurations preserving collective small-displacement motions [34–37]. These collective small-displacement motions bear resemblance to the liquid-like dissipative clusters [31], which provide the microscopic basis for the β' relaxation (also termed fast β, γ, or nearly constant loss), a process widely regarded as a precursor of the β relaxation.

Recent studies have established a close connection between β-relaxation and plastic units, as evidenced by their similar activation energies, the shared temperature–frequency dependence, the ductile–brittle transition, as well as the correlation between stronger β-relaxation and enhanced plasticity [54, 60, 61]. Moreover, yielding and shear-band formation have been associated with the percolation of such plastic units [28]. From this perspective, our double-percolation framework provides microscopic insight into how localized relaxation dynamics develop into macroscopic plastic deformation.

Our findings demonstrate that while the α- and β-relaxations are always associated with percolation of immobile and mobile clusters, respectively, the β-relaxation strength is governed by the extent of configurational changes during these processes. This finding bridges theoretical predictions with experimental observations, offering a unified perspective on relaxation mechanisms in glass-forming systems. The double-percolation framework may be less applicable to polymer, ionic, and molecular glasses, however, in which complex interactions affect percolation and energy dissipation (figure S32), warranting further study.

4. Methods

4.1. Sample preparation

The initial master alloy ingots were prepared by induction melting of elements of purity $\geqslant$ 99.95 at% in a Ti-gettered argon atmosphere in an arc-melting furnace. To ensure chemical compositional homogeneity, all ingots were re-melted at least six times. MG samples, in the form of ribbons approximately 20 μm thick and 1.5 mm wide, were prepared by re-melting part of the initial alloy ingot using induction melting heating of the melts and then injecting them onto the surface of a cold copper roller with the speed of 40–60 m s^{-1} in a high-purity argon atmosphere. Cylindrical samples with diameter 2 mm and length 10 mm were fabricated through suction casting onto a chilled copper mold. The as-prepared amorphous sample was sealed into a quartz tube filled with nitrogen gas to prevent oxidation during heat treatment at different temperatures.

4.2. Dynamical mechanical spectroscopy

Dynamic mechanical experiments were conducted using a dynamic mechanical analyzer (DMA, TA Q-800) with temperature control provided by liquid nitrogen and a nitrogen atmosphere for protection. If the (frequency-dependent) complex Young's modulus E is given by $E = E' + \mathrm{i}E''$ in which E' is the storage modulus and E'' the loss modulus, the loss factor is given by $\tan\delta = E''/E'$. The measurements were performed under tension film mode (samples 78–83, 211–217 and 286 were monitored under single cantilever mode), with a temperature ramping rate of 3 K min^{-1} at different driving frequencies (1, 2, 4, 8, and 16 Hz).

4.3. Molecular dynamics simulations

The initial $Al_{95}Sm_5$ model was first fully melted at 2000 K. To stabilize the liquid structure, the system was then equilibrated isothermally at 900 K for more than 1000 ns. Next, the liquid was cooled to 200 K at two different rates, 100 K ns^{-1} and 0.1 K ns^{-1}, producing fast-cooled and slow-cooled glasses. Finally, both samples were reheated from 200–600 K with heating rate 1 K ns^{-1} to generate representative structures for the DMS simulations.

To numerically replicate the procedure of DMS experiments, a sinusoidal, volume-conserving strain was applied to the simulation box. Specifically, a strain of the form $\varepsilon(t) = \varepsilon_0 \sin(\omega t)$ was imposed at designated time intervals, with the strain amplitude oriented along the xy direction. The induced stress response, $\sigma(t)$, was fitted using $\sigma(t) = \sigma_0 \sin(\omega t + \delta)$. The complex Shear modulus $G = G' + iG''$ were extracted from the relations $G'(\omega) = (\sigma_0/\varepsilon_0)\cos\delta$ and $G''(\omega) = (\sigma_0/\varepsilon_0)\sin\delta$, respectively. To ensure that the material response remained within the linear viscoelastic regime, the deformation amplitude was limited to 1.4%. A time step of 10 fs was chosen to balance numerical stability with computational efficiency. The reported DMS results were obtained by averaging over at least five independent DMS runs.

4.4. Percolation analysis

All particles are classified as either mobile or immobile according to the magnitude of their displacement u during one MD DMS cycle. The critical displacement threshold u_c is determined from the van Hove function, $p(u) \equiv [P(u+\Delta u) - P(u)]/\Delta u$, where $P(u)$ is the cumulative probability of finding a particle with displacement less than or equal to u, normalized such that $\int_0^\infty p(u)\mathrm{d}u = P(\infty) = 1$: the value u_c is defined by the first minimum of $p(u)$. Particles with $u > u_c$ are classified as mobile, while particles with $u < u_c$ by definition are immobile (on the time scale in question, $1/\omega$).

Subsequently, clusters are identified within each of the two classes of mobile and immobile particles, respectively. Two particles are considered part of the same cluster if they belong to the same class and their separation is less than r_c defined as the first minimum of the all-particle radial distribution function $g(r)$.

Acknowledgment

The computational work was carried out on the public computing service platform provided by the Network and Computing Center of HUST. We are thankful for the support of the National Science Foundation of China (52571185).

Data availability statement

All data that support the findings of this study are included within the article (and any supplementary files).

Supporting Information 1 available at https://doi.org/10.1088/1361-6633/aea642/data1.

Supporting Information 2 available at https://doi.org/10.1088/1361-6633/aea642/data2.

Author contributions

Sheng-Hao Zeng
Data curation (equal), Validation (equal), Writing – original draft (equal), Writing – review & editing (equal)

Bo-Yan Wang
Data curation (equal), Writing – original draft (equal), Writing – review & editing (equal)

Liang Gao 0009-0000-2926-7364
Data curation (equal), Writing – original draft (equal), Writing – review & editing (equal)

Qun Yang 0000-0002-4096-3392
Data curation (equal)

Jun-Ying Jiang 0000-0001-6760-3664
Data curation (equal), Software (equal)

Zi-Yi Ren
Data curation (equal)

Jeppe C Dyre 0000-0002-0770-5690
Conceptualization (supporting), Methodology (equal), Writing – review & editing (equal)

Hai-Bin Yu 0000-0003-0645-0187
Conceptualization (lead), Funding acquisition (equal), Methodology (equal), Resources (equal), Supervision (equal), Writing – original draft (equal), Writing – review & editing (equal)

References

[1] Berthier L and Reichman D R 2023 *Nat. Rev. Phys.* **5** 102–16
[2] Berthier L and Biroli G 2011 *Rev. Mod. Phys.* **83** 587–645
[3] He S *et al* 2020 *Sci. Adv.* **6** eaaz8423
[4] Manoharan V N 2015 *Science* **349** 1253751
[5] Lunkenheimer P, Loidl A, Riechers B, Zaccone A and Samwer K 2023 *Nat. Phys.* **19** 694–9

[6] Cubuk E D et al 2017 Science 358 1033–7
[7] Ruta B, Chushkin Y, Monaco G, Cipelletti L, Pineda E, Bruna P, Giordano V M and Gonzalez-Silveira M 2012 Phys. Rev. Lett. 109 165701
[8] Wang Q, Zhang S T, Yang Y, Dong Y D, Liu C T and Lu J 2015 Nat. Commun. 6 7876
[9] Wang W H 2019 Prog. Mater. Sci. 106 100561
[10] Luo P, Li Y Z, Bai H Y, Wen P and Wang W H 2016 Phys. Rev. Lett. 116 175901
[11] Wu Z W, Kob W, Wang W H and Xu L 2018 Nat. Commun. 9 5334
[12] Yu H B, Richert R and Samwer K 2017 Sci. Adv. 3 e1701577
[13] Nishikawa Y, Ozawa M, Ikeda A, Chaudhuri P and Berthier L 2022 Phys. Rev. X 12 021001
[14] Wagner H, Bedorf D, Küchemann S, Schwabe M, Zhang B, Arnold W and Samwer K 2011 Nat. Mater. 10 439–42
[15] Krausser J, Samwer K H and Zaccone A 2015 Proc. Natl. Acad. Sci. vol 112 13762–7
[16] Tanaka H, Tong H, Shi R and Russo J 2019 Nat. Rev. Phys. 1 333–48
[17] Guiselin B, Scalliet C and Berthier L 2022 Nat. Phys. 18 468–72
[18] Spieckermann F et al 2022 Nat. Commun. 13 127
[19] Hu Y C and Tanaka H 2022 Nat. Commun. 13 4519
[20] Zhou Z Y, Yang Q and Yu H B 2024 Prog. Mater. Sci. 145 101311
[21] Coslovich D 2025 Nat. Phys. 21 346–7
[22] Luo P, Wen P, Bai H Y, Ruta B and Wang W H 2017 Phys. Rev. Lett. 118 225901
[23] Wang Z and Wang W H 2018 Natl. Sci. Rev. 6 304–23
[24] Gao L, Sun Y and Yu H B 2023 Phys. Rev. B 108 014201
[25] Dyre J C 2024 J. Phys. Chem. Lett. 15 1603–17
[26] Gao L, Yu H B, Schrøder T B and Dyre J C 2025 Nat. Phys. 21 471–9
[27] Caporaletti F, Capaccioli S, Valenti S, Mikolasek M, Chumakov A I and Monaco G 2021 Nat. Commun. 12 1867
[28] Ghosh A, Budrikis Z, Chikkadi V, Sellerio A L, Zapperi S and Schall P 2017 Phys. Rev. Lett. 118 148001
[29] Saberi A A 2015 Phys. Rep. 578 1–32
[30] Hecksher T, Torchinsky D H, Klieber C, Johnson J A, Dyre J C and Nelson K A 2017 Proc. Natl. Acad. Sci. 114 8710–5
[31] Yu H B and Wang Q 2024 Next Mater. 3 100168
[32] Cicerone M T, Zhong Q and Tyagi M 2014 Phys. Rev. Lett. 113 117801
[33] Zhu F, Nguyen H K, Song S X, Aji D P B, Hirata A, Wang H, Nakajima K and Chen M W 2016 Nat. Commun. 7 11516
[34] Caporaletti F, Capaccioli S, Bessas D, Chumakov A I, Martinelli A, Dallari F and Monaco G 2026 Nat. Phys. 22 1298–305
[35] Saito M, Araki T, Onodera Y, Ohara K, Seto M, Yoda Y and Wakabayashi Y 2025 Acta Mater. 284 120536
[36] White R P, Napolitano S and Lipson J E 2025 Phys. Rev. Lett. 134 098203
[37] Nguyen H K, Shundo A, Yamamoto S, Tanaka K and Nakajima K 2026 Commun. Mater. (https://doi.org/10.1038/s43246-026-01305-8)
[38] Karmakar S, Dasgupta C and Sastry S 2014 Annu. Rev. Condens. Matter Phys. 5 255–84
[39] Qiao J C, Wang Q, Pelletier J M, Kato H, Casalini R, Crespo D, Pineda E, Yao Y and Yang Y 2019 Prog. Mater. Sci. 104 250–329
[40] Pica Ciamarra M, Ji W and Wyart M 2024 Proc. Natl. Acad. Sci. 121 e2400611121
[41] Chacko R N, Landes F P, Biroli G, Dauchot O, Liu A J and Reichman D R 2021 Phys. Rev. Lett. 127 048002
[42] Ozawa M and Biroli G 2023 Phys. Rev. Lett. 130 138201
[43] Starr F W, Douglas J F and Sastry S 2013 J. Chem. Phys. 138 12A541
[44] Paluch M, Wojnarowska Z and Hensel-Bielowka S 2013 Phys. Rev. Lett. 110 015702
[45] Guiselin B, Tarjus G and Berthier L 2022 J. Chem. Phys. 156 194503
[46] Chang C, Zhang H P, Zhao R, Li F C, Luo P, Li M Z and Bai H Y 2022 Nat. Mater. 21 1240–5
[47] Yu H B, Gao L, Gao J Q and Samwer K 2024 Natl. Sci. Rev. 11 nwae091
[48] Jiang J Y, Fan Y W, Gao L and Yu H B 2026 Newton 100624
[49] Ding Y, Shi F, Wang X, Bai Y, Wang Z and Hu L 2024 Acta Mater. 266 119698
[50] Wang J, Song L, Gao Y, Zang B, Gao M, Huo J, Hu L and Wang J Q 2023 Sci. China Mater. 66 3706–12
[51] Yu H B, Tylinski M, Guiseppi-Elie A, Ediger M D and Richert R 2015 Phys. Rev. Lett. 115 185501
[52] Cheng Y et al 2022 Nat. Commun. 13 7352
[53] Wang Q, Zhang L F, Zhou Z Y and Yu H B 2024 Sci. Adv. 10 eadk2799
[54] Zhou Z Y, Sun Y, Gao L, Wang Y J and Yu H B 2023 Acta Mater. 246 118701
[55] Shiraishi K, Mizuno H and Ikeda A 2023 Proc. Natl. Acad. Sci. vol 120 e2215153120
[56] Caporaletti F, Capaccioli S, Valenti S, Mikolasek M, Chumakov A I and Monaco G 2019 Sci. Rep. 9 14319
[57] Tahaei A, Biroli G, Ozawa M, Popović M and Wyart M 2023 Phys. Rev. X 13 031034
[58] Lemaitre A 2014 Phys. Rev. Lett. 113 245702
[59] Sun Y, Peng S X, Yang Q, Zhang F, Yang M H, Wang C Z, Ho K M and Yu H B 2019 Phys. Rev. Lett. 123 105701
[60] Yu H B, Wang W H and Samwer K 2013 Mater. Today 16 183–91
[61] Yang Q, Pei C Q, Yu H B and Feng T 2021 Nano Lett. 21 6051–6